Biosensors and Bioelectronics 94 (2017) 616–625

Contents lists available at ScienceDirect

Biosensors and Bioelectronics

journal homepage: www.elsevier.com/locate/bios

Ultrasensitive electrochemical biosensing platform based on spherical silicon dioxide/molybdenum selenide nanohybrids and triggered Hybridization Chain Reaction

Hong-Lei Shuai[a,c], Xu Wu[b,c], Ke-Jing Huang[a,c,*], Zi-Bo Zhai[a,c]

[a] College of Chemistry and Chemical Engineering, Xinyang Normal University, Xinyang 464000, China
[b] School of Physics and Electronic Engineering, Xinyang Normal University, Xinyang 464000, China
[c] Institute for Conservation and Utilization of Agro-bioresources in Dabie Mountains, Xinyang Normal University, Xinyang 464000, China

ARTICLE INFO

Keywords:
Spherical silicon dioxide/molybdenum selenide
Hybridization Chain Reaction
Sandwich-type
Electrochemical biosensor
Signal amplification
Graphene oxide–gold nanoparticles

ABSTRACT

An ultrasensitive sandwich-type electrochemical biosensor for DNA detection is developed based on spherical silicon dioxide/molybdenum selenide (SiO_2@$MoSe_2$) and graphene oxide–gold nanoparticles (GO–AuNPs) hybrids as carrier triggered Hybridization Chain Reaction (HCR) coupling with multi-signal amplification. The proposed sensoring assay utilizes a spherical SiO_2@$MoSe_2$/AuNPs as sensing platform and GO–AuNPs hybrids as carriers to supply vast binding sites. H_2O_2+HQ system is used for DNA detection and HCR as the signal and selectivity enhancer. The sensor is designed in sandwich type to increase the specificity. As a result, the present biosensor exhibits a good dynamic range from 0.1 fM to 100 pM with a low detection limit of 0.068 fM (S/N=3). This work shows a considerable potential for quantitative detection of DNA in early clinical diagnostics.

1. Introduction

Recently, ultrasensitive and high-selective detection of low abundance nucleic acids has attracted considerable interest due to its important role in precaution of genetic or pathogenic diseases, treatment of viral and bacterial infections, and prognosis of cancer (Liu et al., 2016; Zhou et al., 2014). Various analytical technologies, such as chemiluminescence (Wang et al., 2015a, 2011; Li et al., 2017; He et al., 2013), spectrophotometry (Patel et al., 2016), fluorescence (Ye et al., 2016; Wang et al., 2014a; Wei et al., 2016; Zhu et al., 2015), surface enhanced Raman scattering (Duan et al., 2015; Li et al., 2013) and electrochemical methods (Li et al., 2016; Wang et al., 2015b, 2014b; Yuan et al., 2016) have been used for DNA detection. Among these methods, electrochemical DNA sensors have received particular attention owing to the superior features of low cost, simple, portable and rapid response (Wan et al., 2013; Yao et al., 2013; Yu et al., 2016). Many signal amplification strategies have been used in electrochemical biosensor construction for improving the sensitivity of target DNA detection (Yu et al., 2016). Hybridization Chain Reaction (HCR) is one of the most important (Shuai et al., 2016a; Li et al., 2015; Guo et al., 2016; Trifonov et al., 2016). In the process of HCR, target acts as an initiator to trigger the hybridization reaction, issuing in the formation of long-range DNA sequence in a long nicked duplex DNA. The initiator triggered reaction and generates a low pseudo-positive result, leading to a high signal to noise ratio. In addition, every target can trigger a HCR event and form a long-range DNA sequence. These advantages exhibit great potential in the sensitive detection of DNA.

Nanomaterials with many specific properties have been widely applied in the field of DNA detection. Two-dimensional (2D) transition metal dichalcogenides, such as MoS_2, WS_2, CoS_2 and VS_2, can be good choices due to their large specific surface areas, good electrical conductivity and chemical stability (Huang et al., 2016, 2014). As a typical 2D layered material, MoS_2 can provide short ion diffusion length and large exposed surface area, and therefore has received considerable attention for electrochemical applications (Huang et al., 2014; Farimani et al., 2014). However, the electrical conductivity of MoS_2 is not that good, and $MoSe_2$ with the similar layered structure might be a better candidate. $MoSe_2$ has a higher intrinsic electrical conductivity than MoS_2 due to the more metallic nature of Se, and the unsaturated Se-edges in $MoSe_2$ are also found to be electrocatalytically active (Kong et al., 2013; Wang et al., 2013). However, because of the high surface energy and interlayer Van der Waals attraction, restacking of $MoSe_2$ nanosheets is almost unescapable in practical applications, which greatly reduces the effective specific surface area, and therefore weakens its performance in some degree (Chhowalla et al., 2013; Hwang et al., 2011). So, assembling primordial 2D $MoSe_2$ nanosheets

* Corresponding author at: College of Chemistry and Chemical Engineering, Xinyang Normal University, Xinyang 464000, China.
E-mail address: kejinghuang@163.com (K.-J. Huang).

http://dx.doi.org/10.1016/j.bios.2017.03.058
Received 14 January 2017; Received in revised form 22 March 2017; Accepted 27 March 2017
0956-5663/ © 2017 Published by Elsevier B.V.

onto a template is very significative. In the past few years, SiO_2 nanospheres have been researched extensively for its unique properties including high surface area, inertness, low cost, good hydrophility, simple preparation process, easy surface functionalization, and good biocompatibility (Chen et al., 2015; Ensafi et al., 2016).

Graphene oxide (GO) has high surface area, good water dispersibility and biocompatibility and has been widely used in the construction of electrochemical biosensors (Tung et al., 2016; Shuai et al., 2016b; Borisova et al., 2016). AuNPs are always utilized as conductive enhancer due to its good conductivity. So, GO–AuNPs hybrid will be very suitable to be a signal amplification carrier. This hybrid will greatly improve the probe capacity and heighten the electron mobility, thus enhance the detection sensitivity of the fabricated biosensor.

Herein, an ultrasensitive sandwich-type electrochemical biosensor for DNA detection is developed based on spherical SiO_2@$MoSe_2$ and GO–AuNPs hybrids. Triggered HCR, enzyme and the catalytic reaction of hydrogenperoxide+hydroquinone system are used for signal amplification. Spherical SiO_2@$MoSe_2$ with high surface area and good conductivity are utilized as sensing substrate, which can load more AuNPs to immobilize capture probe and accelerate the electron transfer rate. GO–AuNPs hybrids act as signal amplification carrier can supply abundant Au-S binding sites to conjugate probe DNA. When the target DNA shows up, HCR will occur between auxiliary DNA and bio-H1–bio-H2 (H1–H2), resulting in signal amplification. In addition, horseradish peroxidase (HRP) enzymes are also immobilized on the electrode as a signal indicator via specific binding of avidin-biotin. Signal-amplification can be further achieved through the catalytic reaction of hydrogenperoxide+hydroquinone (H_2O_2+HQ) system. Therefore, combining the above advanced aspects together, the proposed assay shows ultrahigh sensitivity and selectivity for target DNA detection.

2. Experimental section

2.1. Reagents and materials

Graphite powder, selenium powder, concentrated ammonia solution, hydrazine hydrate, tetraethoxysilane (TEOS), $Na_2MO_4{\cdot}2H_2O$, urea and chloroauric acid ($HAuCl_4{\cdot}3H_2O$) were obtained from Aladdin Chemicals Co. Ltd. (Shanghai, China). 6-mercaptohexanol (MCH) was purchased from Sigma-Aldrich (Shanghai, China). Water was purified with a Milli-Q purification system (≥18 MΩ, Millipore). Horseradish peroxidase (HRP) and all DNA sequences were synthesized by Shanghai Sangon Biological Engineering Technology Co. Ltd. (Shanghai, China) and their sequences were as follows:

Capture probe: 5’ -ACGGAAACTGCAAGTATTTTT-(CH2)3-SH -3’
Probe DNA: 5’-SH - (CH2)6-TGCAGTTTCCGTCCGTAGTTTTT -3’
Target DNA: 5’-CTACGGACGGAAACTGCACCTGTATTCCCATACCCATCAT-3’
One-based mismatch DNA: 5’-CTACGGACGGAAACTGCAACTGTATTCCCATACCCATCAT-3’
Three-based mismatch DNA: 5’-CTACGGACGCAAACTGCAACTGTATTCTCATACCCATCAT-3’
Noncomplementary: 5’-CTGCTTCCAAACCTTTAACATAGCCGCAAGCGTTAGCTGC-3’
Auxiliary DNA: 5’-AGTCTAGGATTCGGCGTGGGTTAAATGATGGGTATGGGAATACAGG-3’
Bio-H1: 5’-biotin-TTAACCCACGCCGAATCCTAGACTCAAAGTAGTCTAGGATTCGGCGTG-3’
Bio-H2: 5’-biotin-AGTCTAGGATTCGGCGTGGGTTAACACGCCGAATCCT

The buffers used in this work are shown in Table 1.

Table 1
Buffers used in this work.

No.	Buffer	Application
1	PBS1 (10 mM PBS, 3 M NaCl and 2.7 mM KCl, pH 7.4)	Capture DNA, Probe DNA
2	PBS2 (10 mM PBS, 150 mM NaCl, 2.7 Mm KCl and 10 mM MgCl2, pH 7.4)	Target DNA, Auxiliary DNA, Mismatch DNA
3	PBS3 (50 mM PBS and 1 M NaCl, pH 7.4)	Bio-H1, Bio-H2

2.2. Apparatus

Cyclic Voltammetry (CV) and differential pulse voltammetry (DPV) were tested on an EC550 electrochemical workstation (Wuhan, Gaoss Union, China) and electrochemical impedance spectroscopy (EIS) measurements were carried out on a RST5200F electrochemical workstation (Zhengzhou Shi Rui Si Instrument, China) with a conventional three-electrode system composed of a platinum wire as an auxiliary electrode, a saturated calomel electrode (SCE) as a reference electrode and a 3-mm diameter GCE as a working electrode. Nanostructures were characterized by a JEM 2100 transmission electron microscope (TEM, JEOL, Tokyo, Japan) and a Hitachi S-4800 scanning electron microscope (SEM, Tokyo, Japan). The BET specific surface areas of the samples were analyzed by using a nitrogen adsorption apparatus (ASAP2460 4MP, China). X-ray diffraction (XRD) pattern was operated on a model D/max-rA diffractometer (Rigaku, Japan). Raman spectra were recorded at ambient temperature on a Renishaw Raman system model 1000 spectrometer (Gloucestershire, UK).

2.3. Preparation of GO–AuNPs hybrids

Graphene oxide (GO) was prepared through modified Hummers’ method. GO–AuNPs carrier was prepared according to a previous protocol (Goncalves et al., 2009). Firstly, 25 mL of 0.48 mM $HAuCl_4$ solution and 1.25 mL of 1 mg/mL GO solution were mixed and stirred for 30 min at room temperature. After that, the mixture was heated to 80 °C, and 470 μL of 85 mM sodium citrate was then added into the solution slowly and stirred for 60 min. Finally, the sample was obtained after the reaction mixture was centrifugally (5 min, 8000 rpm) washed with water and dried in drying oven at 60 °C.

Typical immobilization of DNA on GO–AuNPs hybrids were as follow (Wang et al., 2016): firstly, probe DNA (20 μL, 100 μM) were mixed with 1 mL GO–AuNPs solution and incubated for at 4 °C 48 h. Next, the mixture was centrifuged for 10 min at 8000 rpm. The precipitate was washed with 10 mM PBS (pH=7.0) for several times and then dispersed in 1 mL of 10 mM PBS (pH=7.0).

2.4. Synthesis of spherical SiO_2@$MoSe_2$

In order to obtain spherical $MoSe_2$, SiO_2 was firstly prepared as template. 24.8 mL water and 90 mL concentrated ammonia solution were mixed to obtain solution A. 61.8 mL absolute ethyl alcohol and 4.5 mL TEOS were mixed uniformly to obtain solution B. Then, solution B was dropwise added into solution A under vigorous stirring for 2 h. The white precipitate of SiO_2 was centrifugally washed with water and ethyl alcohol, and finally dried in drying oven at 60 °C.

To grow hierarchical $MoSe_2$ shell on SiO_2 sphere template, 0.05*g* of the as-prepared SiO_2 sphere was ultrasonically dispersed into a mixture of 20 mL water and 30 mL ethyl alcohol. Then, 0.21g sodium molybdate ($Na_2MoO_4{\cdot}2H_2O$) was added and ultrasonic for 10 min. After that, 0.18g selenium powder which was dissolved in 10 mL hydrazine hydrate was added to the reaction solution. At last, the mixture was transferred into a 100 mL Teflon-lined stainless steel autoclave and sustained in an oven at 200 °C for 24 h. The black precipitate of SiO_2@

$MoSe_2$ core-shell sphere was collected by centrifugation, washed thoroughly with ethanol, and dried at 60 °C for 12 h.

2.5. Preparation of biosensor and electrochemical measurements

Prior to use, Bio-H1 and Bio-H2 were incubated at 95 °C for 5 min and intermixed in 1:1(v/v) after cooling to room temperature. Before the modification, bare GCE was polished sequentially with 0.3 and 0.05 μm alumina slurries, washed ultrasonically in water and ethanol, and then dried with nitrogen gas. 8.0 μL SiO_2@$MoSe_2$ core-shell sphere suspension (1 mg/mL) was applied onto the cleaned GCE and dried in the air to obtain SiO_2@$MoSe_2$/GCE. To immobilize the capture probe, AuNPs was electrodeposited onto SiO_2@$MoSe_2$/GCE in a PBS (pH 7.0) solution containing 0.1% $HAuCl_4$ at a constant potential of −0.2 V for 45 s. After that, 8 μL thiolated capture probe (1×10^{-6} M) was cast on the AuNPs/SiO_2@$MoSe_2$/GCE and allowed to react overnight. After thoroughly washed with water, 8 μL MCH (1 mM) were dropped onto the electrode and incubated for 30 min to eliminate nonspecific adsorption. Then, 8 μL DNA-linked Go-AuNPs were applied on the electrode and incubated for 70 min. Again, the electrode was rinsed with water, and 8 μL different concentrations of target DNA was added on the electrode and incubated at 37 °C for 65 min. After that, 8 μL Auxiliary DNA (1 μM) was added on the electrode and incubated at 37 °C for 90 min. Afterward, 8 μL of the mixture (H1-H2) was coated on the resultant electrode and incubated at 37 °C for 70 min for the HCR. Subsequently, 6 μL avidin–HRP (0.5 mM/mL) was dropped on the electrode and incubated at room temperature for 40 min. Thereafter, the resulting electrode was rinsed with water and used for electrochemical measurements.

For miRNA sensing, cyclic voltammetry (CV) was carried out in 0.1 M PBS (pH 7.0) containing 10 mmol L^{-1} $[Fe(CN)_6]^{3-/4-}$ and 0.1 mol L^{-1} KCl solution between a potential window of −0.2 V and 0.6 V with a scan rate of 100 mV s^{-1}. EIS measurements were performed in 0.1 M PBS (pH 7.0) containing 5.0 mmol L^{-1} $[Fe(CN)_6]^{3-/4-}$ and 0.1 mol L^{-1} KCl solution, with the AC voltage amplitude of 5 mV and voltage frequencies from 100 kHz to 0.1 Hz at the applied potential of 0.2 V. The DPV measurements were conducted in the potential region from −0.4 V to 0.2 V (vs. SCE) in 0.1 M PBS (pH 7.0) containing 2 mM HQ and 1.8 mM H_2O using a pulse amplitude of 50 mV, pulse width of 50 ms and pulse period of 0.2 s.

3. Results and discussion

3.1. Design principle of the biosensor

Fabrication principle of the proposed sandwich-type DNA biosensor is illustrated in Scheme 1. Firstly, thiol modified capture probes which are partial-complementary with probe DNA are fixed on AuNPs/SiO_2@$MoSe_2$ modified electrode. Then, MCH was dropped onto the electrode to block the unreacted gold surface. Subsequently, DNA-linked GO–AuNPs hybrids carrier are introduced to hybridize with capture probe and a sandwich-type structure is formed. GO–AuNPs hybrids bring large amounts of probe DNA to electrode, which strands on AuNPs to capture target DNA. After that, introduction of auxiliary DNA can hybridize with target DNA, and the two species of DNA hairpins bio-H1 and bio-H2 are opened by the auxiliary DNA to trigger HCR reaction. Since two hairpins are modified with biotin, HRP is immobilized through the streptavidin–biotin reaction to further amplify the signal. Finally, DPV is tested in hydrogen peroxide+hydroquinone solution. Thus, the proposed strategy effectively combines the advantages of spherical SiO_2@$MoSe_2$ nanomaterials, GO–AuNPs carrier, HRP signal amplification strategy, hydrogen peroxide+hydroquinone detection system and sandwich-type structure, and eventually shows high sensitivity and good selectivity for target DNA detection.

3.2. Materials characterization

The XRD patterns of the as-prepared GO-AuNPs, SiO_2 templates and SiO_2@$MoSe_2$ composites are shown in Fig. 1. As shown in Fig. 1A, GO shows a sharp peak at 10.3° (001). For GO-AuNPs, additional peaks can be observed at 38.6°, 44.8°, 64.2°, and 77.4°, which are corresponding to the (111), (200), (220), and (311) crystal planes of AuNPs, respectively. From Fig. 1B, SiO_2 templates exhibit a broad peak at around 23.38°. For SiO_2@$MoSe_2$, except the peak at around 23.38°, high-intensity peaks at 14.7°, 33.26° and 54.52° can also be found, which are in accordance well with the (002), (100) and (110) planes of $MoSe_2$ (JCPDS: 29-0914).

Raman spectra of various materials are recorded and the results are displayed in Fig. 1C and D. In Fig. 1C, peaks at 1350 and 1590 cm^{-1} are corresponding to the typical peaks of *D* band and *G* band of GO, respectively. The *D* bands originate from the lattice destruction of sp^2-hybridized carbon and the *G* bands arise from the first-order scattering of the E_{2g} mode. It can be obviously seen that AuNPs can enhance the Ranman scattering signal due to AuNPs has a property which is called SERS. It can capture the lights and focus them contributing to the increase of the intensity of *D* and *G* band. From Fig. 1D, four characteristic peaks can be found for SiO_2. Peaks at 200 cm^{-1}, 818 cm^{-1} and 1000 cm^{-1} are corresponding to the symmetric Si-O stretching vibrations and a band at 663 cm^{-1} associate with the Si-O-Si bending modes of bridging oxygens (Retsinas et al., 2016). The other two peaks at 241 and 293 cm^{-1} are related to the existence of $MoSe_2$. The result is in accord with the XRD result in Fig. 1B, suggesting the successful synthesis of SiO_2@$MoSe_2$.

XPS was performed to characterize the chemical composition of the samples. The XPS spectrum of SiO_2@$MoSe_2$ was shown in Fig. 1E, revealing the presence of the element Si, O, Se and Mo in the SiO_2@$MoSe_2$ sample. The atomic concentrations (at%) of Si, O, Mo and Se are calculated from XPS spectra of SiO_2@$MoSe_2$. The element content of Si, O, Mo and Se are 24.16%, 47.72%, 9.23% and 18.89%, respectively. The calculated atomic ratio of O to Si element is 1.98 and Se to Mo element is 2.05, approaching the theoretical stoichiometric value of SiO_2 and $MoSe_2$.

Morphology of the as-obtained SiO_2 templates, SiO_2@$MoSe_2$ and GO-AuNPs are characterized with SEM and TEM. SEM images of SiO_2 templates in Fig. 2A and B show that the SiO_2 templates possess a uniformly spherical structure with an average diameter of about 250 nm. The low diameter distribution of the templates ensures the uniform coating of $MoSe_2$. Fig. 2C and D are the SEM images of SiO_2@$MoSe_2$, it can be found that the SiO_2 templates are homogeneously coated with $MoSe_2$ nanosheets, which enables the large specific area and highly porous channels of the composite. From the TEM images of SiO_2 (Fig. 2E) and SiO_2@$MoSe_2$ (Fig. 2F and its inset), it can be more clearly seen that the SiO_2 is evenly wrapped by $MoSe_2$ nanosheets. Fig. 2G is an enlarged SEM image of SiO_2@$MoSe_2$, showing ultrathin $MoSe_2$nanosheets stretching out of the sphere. From the HRTEM image in Fig. 2H, lattice fringes are found on the $MoSe_2$ nanosheets, and the d-spacing of 0.64 nm can be assigned to the (002) lattice plane of hexagonal $MoSe_2$. Moreover, the elemental mapping of SiO_2@$MoSe_2$ is shown in Fig. 2I. It can be clearly seen that the O, Si, Se, and Mo elements are uniformly and continuously distributed in SiO_2@$MoSe_2$ samples. TEM image of GO-AuNPs is displayed in Fig. 2J. It can be clearly seen that the AuNPs are well dispersed on GO, and the average diameter of AuNPs is about 18 nm. Brunauer–Emmett–Teller (BET) specific surface area and porosity of SiO_2@$MoSe_2$ spheres are studied by nitrogen adsorption–desorption analysis (Fig. 2K). The results show the BET specific surface area of the SiO_2@$MoSe_2$ spheres is 87.36 m^2 g^{-1}. The pore size distribution shown in the inset demonstrates the pore diameters of SiO_2@$MoSe_2$ is about 2.4 nm. This can provide a large space for the deposition of AuNPs and the subsequent immobilization of capture probe, which are quite beneficial to the construction of high-performance biosensor.

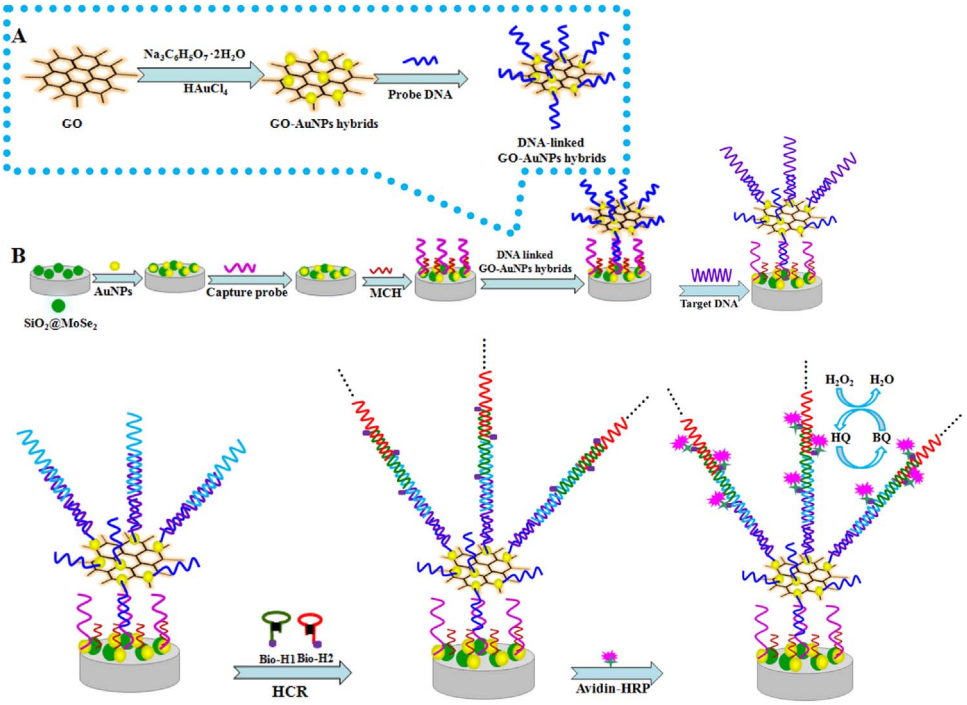

Scheme 1. Schematic illustration of the DNA biosensor based on spherical SiO_2@$MoSe_2$ and GO–AuNPs hybrids as carrier triggered HCR coupling with multi-signal amplification.

The particle size distribution was measured by using a laser particle size analyzer (MasterSizer 2000, Malvern, UK). As shown in Fig. 2L, different particle size fractions of SiO_2@$MoSe_2$ spheres were gained from 260 nm to 300 nm. The majority of particle are concentrated in 270–209 nm, nonetheless, 208 nm particle volume fraction is 63.5%, indicating the particle sizes of SiO_2@$MoSe_2$ spheres are about 280 nm.

The elemental composition of the SiO_2@$MoSe_2$ is detected by EDAX analysis as shown in Fig. 2M. The spectrum shows that the samples were composed of Mo, Se, Si and O peaks. As shown in inset, the atomic ratio of Mo to Se was calculated as approximately 1:2 and O to Si element is near 2:1, indicating the successful decoration of the surface of SiO_2 with $MoSe_2$ nanosheets. The mass fraction of SiO_2 and $MoSe_2$ in the composites can be ascertained to be around 21% and 79%, respectively.

3.3. Electrochemical characterization

CV was used to characterize different modified electrodes (Fig. 3). As is shown in Fig. 3A, the bare GCE displays a pair of well-defined redox peaks in $[Fe(CN)_6]^{3-/4-}$ solution (curve a). The peak currents slightly increase (curve b) when SiO_2@$MoSe_2$ sphere are applied on GCE, due to the high surface area of SiO_2@$MoSe_2$. When AuNPs are further modified on the electrode, the current response enhances greatly (curve c), mainly owing to the high conductivity of AuNPs which can accelerate the electron transfer rate to take full advantage of the large specific surface area of SiO_2@$MoSe_2$ sphere. From Fig. 3B, we can found that the current responses decrease greatly (curve d) when capture probe is modified on the above electrode, this is because the capture probe hinders the diffusion of ferricyanide toward the electrode surface. Similarly, the current response decreases again (curves e) after MCH is coated on the electrode. This may come from the fact that MCH insulates the conductive support and the electron transfer becomes more difficult. However, the peak currents prodigiously increase (curve f) after the immobilization of DNA-linked GO-AuNPs hybrids, due to the large specific surface area of GO and the conductive AuNPs can highly accelerate the electron transfer rate. The peak currents gradually decrease when target DNA, auxiliary DNA, H1-H2 and HRP (curve g, h, i and j) are subsequently modified on the electrode, because the extension of negatively charged DNA chains hinders the electron transfer. The above CV results suggested the successful construction of the biosensor.

EIS is another practical method to characterize the modified electrodes. Diameter of the semicircle in the resulting pattern can indexes the interfacial electron transfer resistance (R_{et}) of the electrode. Figs. S1A and 1B display the feature EIS results of the electrodes after different modification processes. We can see that the bare GCE (curve a) has the largest R_{et} value. The R_{et} decreases obviously with the coating of SiO_2@$MoSe_2$ sphere (curve b) and the deposition of AuNPs (curve c), indicating the enhancement of the electron conductivity by the synergistic effect of AuNPs and SiO_2@$MoSe_2$. While, after the modification of capture probe (curve d) and MCH (curves e), R_{et} values obviously increase. The value decreases after the introduction of the mixture of DNA-linked GO-AuNPs hybrids (curve f). When target DNA (curve g), axially DNA (curve h), H1-H2 (curve i) and HRP (curve j) are introduced on the electrode, the R_{et} value gradually increases, respectively. We can find that the EIS results agree well with the CV performances shown in Figs. 3A and B, further reveals the successful fabrication of the biosensor.

The effective surface area (A) of electrodes were evaluated by chronocoulometry in 0.1 mM $K_3[Fe(CN)_6]$ solution containing 1.0 M KCl, according to the equation as follows:

$$Q = 2nFAcD^{1/2}t^{1/2}/\pi^{1/2} + Q_{dl} + Q_{ads} \quad (1)$$

where n, F, c, Q_{dl} and Q_{ads} (C) are the number of electron transferred, Faraday constant, concentration of substrate, diffusion coefficient, double layer charge and adsorption charge, respectively. The other symbols have their usual significances. As is shown in Figs. 3C and D, from the slope value of the obtained curves, A is calculated to be 0.016 cm^2 for bare GCE and 0.089 cm^2 for AuNPs/SiO_2@$MoSe_2$/GCE. This indicates that the effective surface area of the electrode is enhanced for nearly 6 times after modified with AuNPs/SiO_2@$MoSe_2$ film. Fig. 3E shows the signal-amplification effect of the as-prepared material. From curves a and b, we can see the current signal increases by 292.3% (signal gain) after the SiO_2@$MoSe_2$ sphere is introduced to the biosensor.

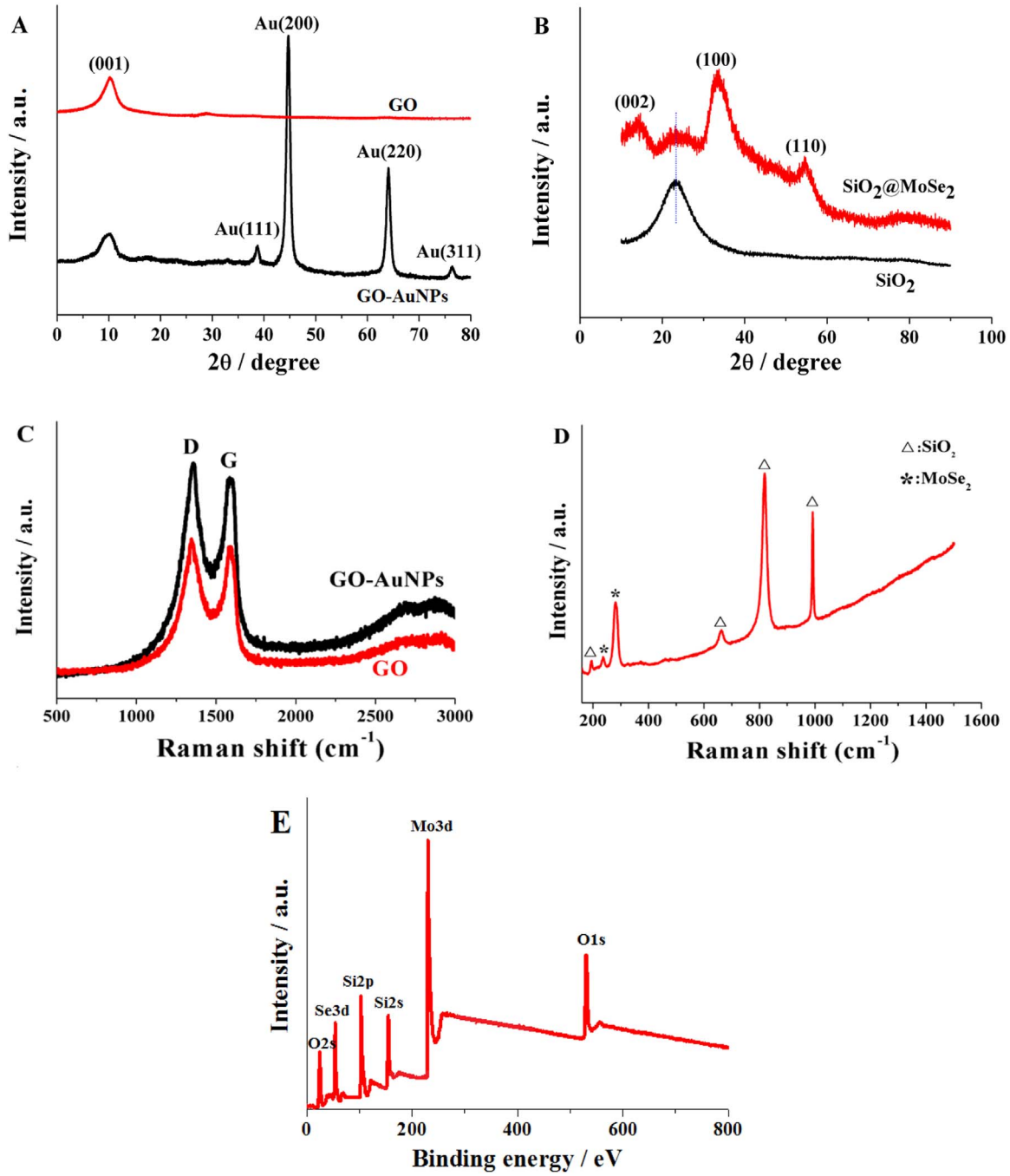

Fig. 1. XRD patterns of GO and GO-AuNPs (A), SiO_2@$MoSe_2$ (B); Raman spectra of GO and GO-AuNPs (C), SiO_2@$MoSe_2$ (D) and XPS spectrum of SiO_2@$MoSe_2$ (E).

3.4. Optimization of experimental conditions

To obtain the best analytical performance, several experimental conditions were optimized. The effect of deposition time of AuNPs on the current response was tested in the range of 10–100 s, with the results shown in Fig. S2A. The peak currents increase with the deposition time extend to 45 s and the current response decreases gradually after 45 s. This is because the conductivity will be enhanced as more and more AuNPs are formed on the electrode surface at the starting stage (10–45 s), while there are too much AuNPs after 45 s and the active sites will be reduced. So the optimizing deposition time of 45 s was used.

The effect of the incubation time of capture probe and DNA-linked GO-AuNPs hybrids was evaluated (Fig. S2B). The current response increases promptly with the incubation time lasts from 20 to 70 min, and it stays stable after 70 min, confirming that the hybridization reaction was accomplished. So 70 min of incubation time was employed.

As shown in Fig. S2C, the hybridization reaction time between probe DNA and target DNA were studied. The peak currents increase rapidly when the reaction time ranges from 20 to 65 min, and remains stable after 65 min, indicating that the hybridization reaction accomplishes at 65 min. Thus, hybridization reaction time of 65 min was used. Similarly, the effect of hybridization reaction time between target DNA and auxiliary DNA on current respond was also evaluated. As can be seen from Fig. S2D, the peak currents keep unchange when it exceeds 90 min, so efficient hybridization time is chosen to be 90 min Fig. S2E and S2F show the current responses to HCR time and self-

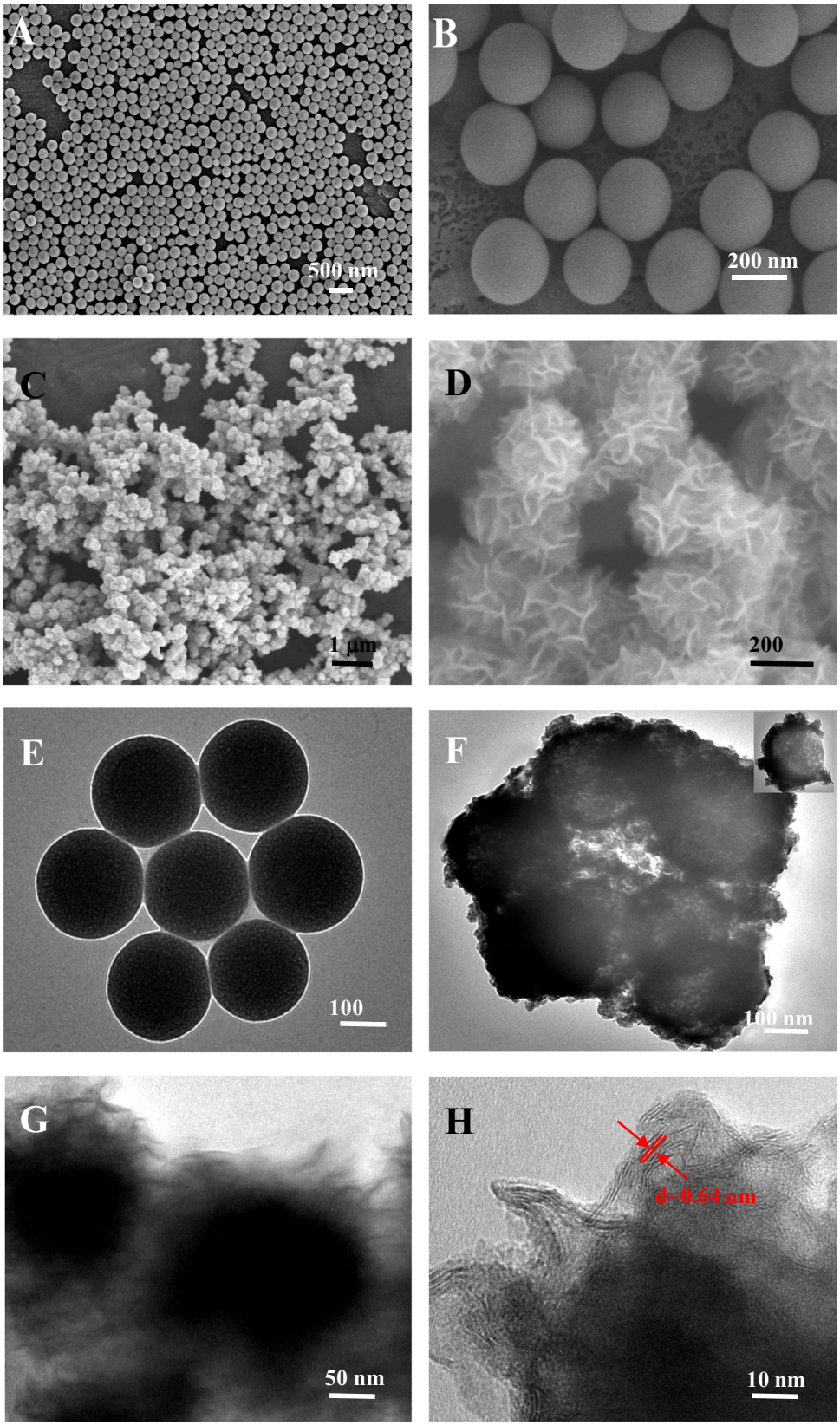

Fig. 2. SEM images of SiO_2 (A, B) and SiO_2@$MoSe_2$ (C, D); TEM images of SiO_2 (E), SiO_2@$MoSe_2$ (F, G), GO-AuNPs (J); HRTEM image of SiO_2@$MoSe_2$ (H); Elemental mapping images of SiO_2@$MoSe_2$ (I); N_2 adsorption-desorption isotherm of the SiO_2@$MoSe_2$ microcubes (K); Results of particle size distribution calculation for SiO_2@$MoSe_2$ (L) and EDAX spectrum of SiO_2@$MoSe_2$ (M).

assembly time of HRP. We can find that the peak current increase stops at 70 min for the HCR, meaning the HCR is primitively completed at that point. For self-assembly of HRP, the largest current indensity comes at 40 min, which reveals that the maximum HRP is immobilized on the electrode at that time. So we consider 70 min for HCR and 40 min for self-assembly of HRP.

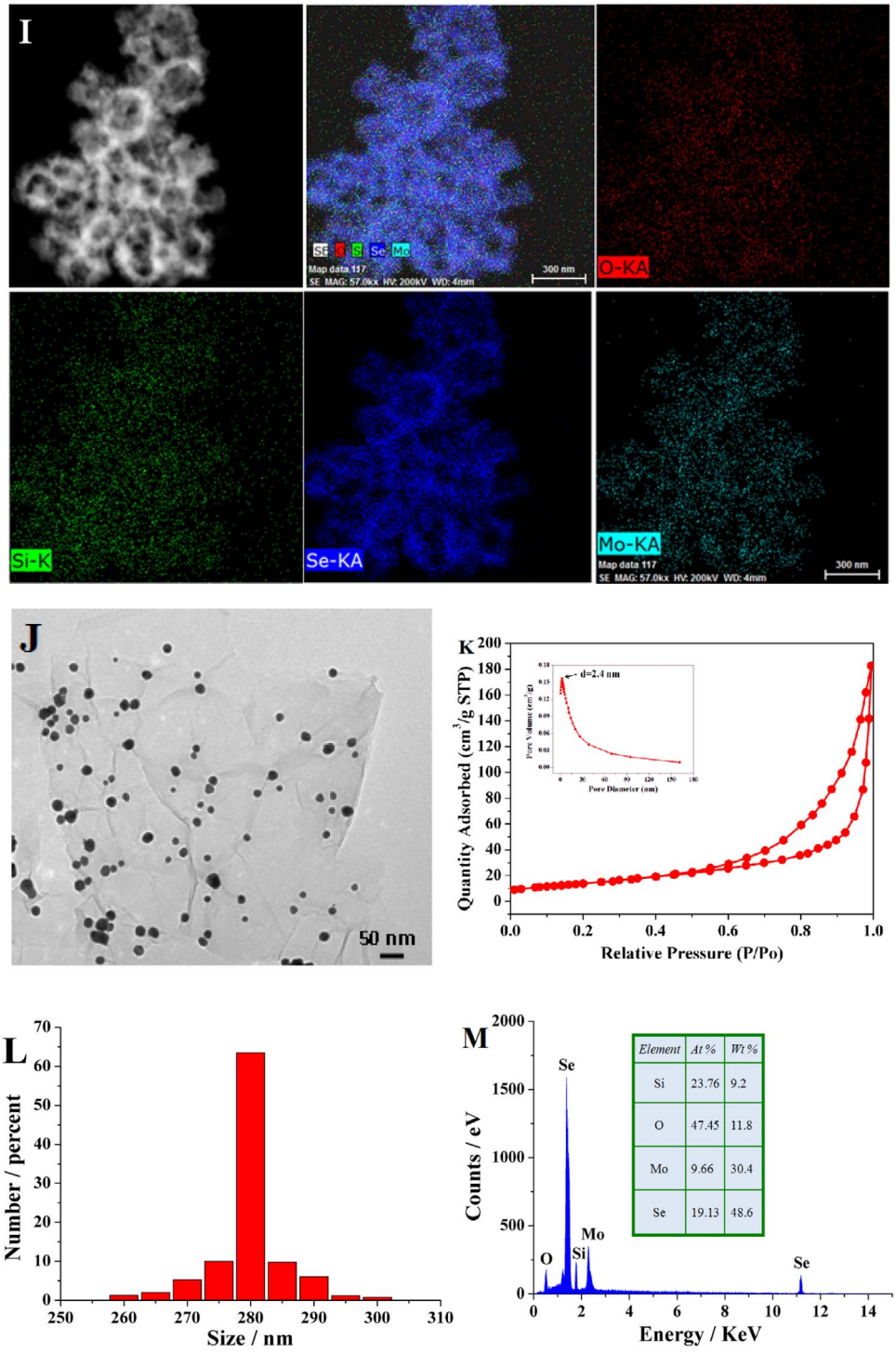

Fig. 2. (*continued*)

3.5. Analytical performance of designed biosensor

The DNA detection was performed by DPV under the optimum conditions. Fig. 4A shows that the peak currents increase with the increasing concentrations of DNA, and a good linear relationship between DPV currents and the logarithm of DNA concentration ranging from 0.1 fM to 100 pM can be obtained (inset of Fig. 4A). The linear calibration equation could be written as $I(\mu A) = -4.69 \log(c/M) - 75.83$ (I is peak current and c is concentration of DNA) with a correlation coefficient (R) of 0.995. The detection limit was 0.068 fM (S/N=3). The analytical performances of different assays for DNA detection are compared in Table S1, and the proposed assay exhibits the lowest detection limit and the widest detection range (Liu et al., 2016; Shuai et al., 2016a; Chen et al., 2016a, 2016b; Hu et al., 2012; Yu et al., 2015).

3.6. Selectivity, reproducibility and stability

The selectivity of the proposed biosensor was investigated by measuring peak current variation with different DNA sequences. Fig. 4B shows the peak current of complementary sequence is the highest, while the peak current of non-complementary sequence and

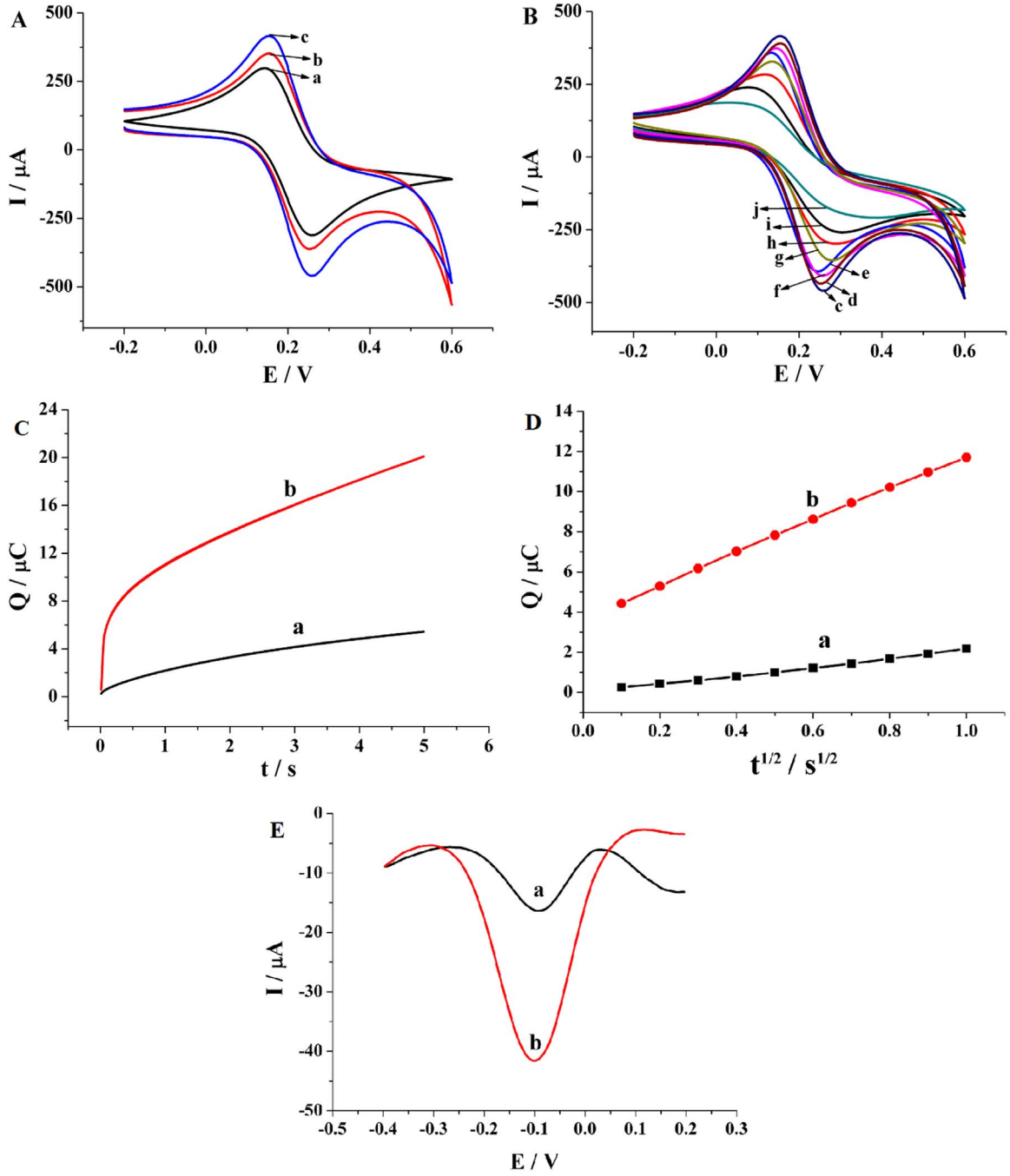

Fig. 3. CVs (A, B) of bare GCE (a), SiO_2@$MoSe_2$/GCE (b), AuNPs/SiO_2@$MoSe_2$/GCE (c), capture probe/AuNPs/SiO_2@$MoSe_2$/GCE/(d), MCH/capture probe/AuNPs/SiO_2@$MoSe_2$/GCE (e), DNA linked GO–AuNPs hybrids/MCH/capture probe/AuNPs/SiO_2@$MoSe_2$/GCE (f), target DNA/DNA linked GO–AuNPs hybrids/MCH/capture probe/AuNPs/SiO_2@$MoSe_2$/GCE (g), Auxiliary DNA/target DNA/DNA linked GO–AuNPs hybrids/MCH/capture probe/AuNPs /SiO_2@$MoSe_2$/GCE (h), HCR/Auxiliary DNA/target DNA/DNA linked GO–AuNPs hybrids/MCH/capture probe/AuNPs/SiO_2@$MoSe_2$/GCE (i), HRP/HCR/Auxiliary DNA/target DNA/DNA linked GO–AuNPs hybrids/MCH/capture probe/AuNPs /SiO_2@$MoSe_2$/GCE (j), CV experiments were conducted in 0.1 M PBS solution containing 1.0 mM $[Fe(CN)_6]^{3-/4-}$ and 0.1 M KCl; (E) Plot of Q-t curves of the bare GCE (a) and AuNPs/SiO_2@$MoSe_2$/GCE (b) in 0.1 mM $K_3[Fe(CN)_6]$ containing 1.0 M KCl; (F) plot of Q-$t^{1/2}$ curves on GCE (a) and AuNPs/SiO_2@$MoSe_2$/GCE (b); (G) DPVs of HRP/HCR/Auxiliary DNA/target DNA/DNA linked GO–AuNPs hybrids/MCH/capture probe/AuNPs/GCE (a) and HRP/HCR/Auxiliary DNA/target DNA/DNA linked GO–AuNPs hybrids/MCH/capture probe/AuNPs/SiO_2@$MoSe_2$ /GCE (b) in 0.1 M PBS (7.0) containing 1.8 mM H_2O_2 and 2 mM HQ.

three-based mismatch sequence is negligible. For single-base mismatched sequence, the peak current is only 3.7% of that of complementary sequence, showing the good selectivity of proposed assay. In addition, five equally prepared electrodes were used to detect 1 pM DNA and the relative standard deviation (RSD) was only 4.2%. Furthermore, the biosensor was kept under 4 °C for 10 days and 93.8% of the initial response to 1 pM DNA can still be remained, suggesting its good stability. Good reproducibility and stability can be attributed to the high specific surface area of spherical SiO_2@$MoSe_2$ and GO-AuNPs hybrids, which can supply more binding sites and strong interaction between enzyme and HCR.

3.7. Real sample analysis

To further investigate the application potential of the developed DNA assay, recovery experiments were implemented by adding different concentration of DNA into the 10-fold diluted healthy human serum sample (obtained from Xinyang Central Hospital, China). Each

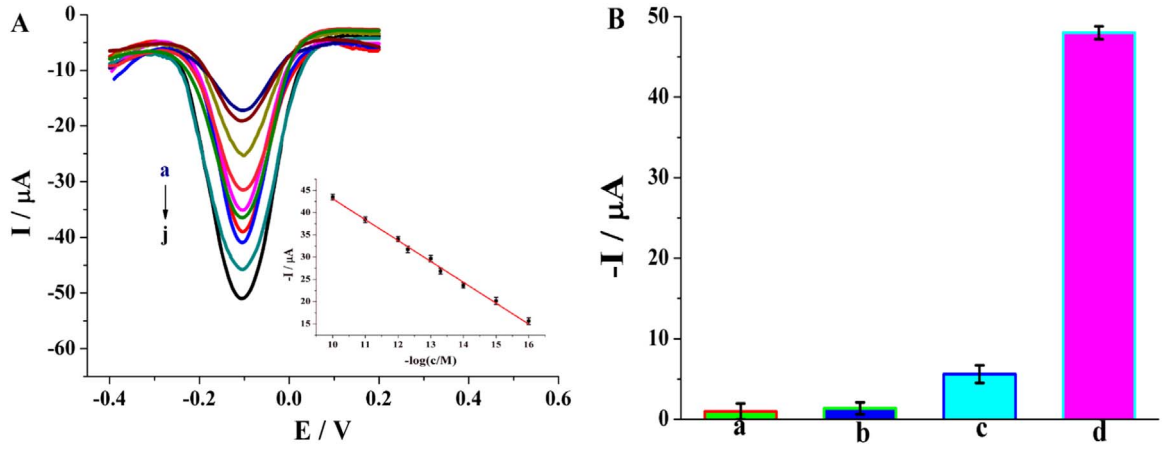

Fig. 4. (A) DPVs of various target DNA concentrations (from a to i): 0, 1.0×10^{-1o}, 1.0×10^{-11}, 1.0×10^{-12}, 5.0×10^{-12}, 1.0×10^{-13}, 5.0×10^{-13}, 1.0×10^{-14}, 1.0×10^{-15}, 1.0×10^{-16} mol/L, respectively. Inset: the calibration plots of the DPV current versus the logarithm concentration of target DNA. Error bars show the standard deviations of measurements taken from three independent experiments; (B) selectivity of the sensor hybridized to different DNA sequences: non-complementary sequence (a), three-based mismatch sequence (b), single-based mismatch sequence (c), and target DNA (d).

sample was detected for three times and the detection value took the average. As is shown in Table S2, recoveries are in the range of 93.0–103.3%, and RSDs are ranging from 3.1 to 6.8, suggesting that the present assay is available for determining DNA in real samples.

4. Conclusions

In summary, we report an ultrasensitive sandwich-type electrochemical biosensor for DNA detection, which is developed based on spherical silicon dioxide/molybdenum selenide with GO–AuNPs hybrids as carrier and triggered HCR for signal amplification. This strategy exhibits an excellent performance for DNA detection with high sensitivity, specificity and repeatability. The main advantages and significance of the biosensor contribute to several aspects. Firstly, spherical SiO_2@$MoSe_2$ has large specific surface area which can load more AuNPs to immobilize capture probe and accelerate the electron transfer rate. Secondly, GO–AuNPs hybrids as carrier can supply vast binding sites to enhance signal response. Thirdly, HCR is a signal amplification tool for enhancing signal response and improving detection selectivity. Fourthly, Hydrogen peroxide+Hydroquinone system is used to detect DNA for improving detection sensitivity and lead to a remarkable lower detection limit (0.068 fM). Finally, sandwich-type strategy greatly increases the specificity and sensitivity of the assay. Therefore, combining these advantages, the proposed biosensor exhibits a high potential for the determination of DNA in clinical applications.

Acknowledgments

This work was supported by the National Natural Science Foundation of China (21475115), Program for University Innovative Research Team of Henan (15IRTSTHN001), Henan Provincial Science and Technology Innovation Team (C20150026), Nanhu Scholars Program of XYNU and Henan Science and Technology Cooperation Project (172106000064).

Appendix A. Supplementary material

Supplementary data associated with this article can be found in the online version at doi:10.1016/j.bios.2017.03.058.

References

Borisova, B., Sánchez, A., Jiménez-Falcao, S., Martín, M., Salazar, P., Parrado, C., Pingarrón, J.M., Villalonga, R., 2016. Sens. Actuators B 232, 84–90.
Chen, H.G., Ren, W., Jia, J., Feng, J., Gao, Z.F., Li, N.B., Luo, H.Q., 2016b. Biosens. Bioelectron. 77, 40–45.
Chen, M., Hou, C.J., Huo, D.Q., Bao, J., Fa, H.B., Shen, C.H., 2016a. Biosens. Bioelectron. 85, 684–691.
Chen, X., Zhang, Q., Qian, C., Hao, N., Xu, L., Yao, C., 2015. Biosens. Bioelectron. 64, 485–492.
Chhowalla, M., Shin, H.S., Eda, G., Li, L.J., Loh, K.P., Zhang, H., 2013. Nat. Chem. 5, 263–275.
Duan, B., Zhou, J.J., Fang, Z., Wang, C.X., Wang, X.J., Hemond, H.F., Chan-Park, M.B., Duan, H.W., 2015. Nanoscale 7, 12606–12613.
Ensafi, A.A., Zandi-Atashbar, N., Rezaei, B., Ghiaci, M., Taghizadeh, M., 2016. Electrochim. Acta 214, 208–216.
Farimani, A.B., Min, K., Aluru, N.R., 2014. ACS Nano. 8, 7914–7922.
Goncalves, G., Marques, P.A.A.P., Granadeiro, C.M., Nogueira, H.I.S., Singh, M.K., Gracio, J., 2009. Chem. Mater. 21, 4796–4802.
Guo, J.J., Wang, J.C., Zhao, J.Q., Guo, Z.L., Zhang, Y.Z., 2016. ACS Appl. Mater. Interfaces 8, 6898–6904.
He, Y., Huang, G.M., Cui, H., 2013. ACS Appl. Mater. Interfaces 5, 11336–11340.
Hu, Y.W., Li, F.H., Han, D.X., Wu, T.S., Zhang, Q.X., Niu, L., Bao, Y., 2012. Anal. Chim. Acta 753, 82–89.
Huang, K.J., Liu, Y.J., Wang, H.B., Wang, Y.Y., Liu, Y.M., 2014. Biosens. Bioelectron. 55, 195–202.
Huang, K.J., Shuai, H.L., Zhang, J.Z., 2016. Biosens. Bioelectron. 77, 69–75.
Hwang, H., Kim, H., Cho, J., 2011. Nano Lett. 11, 4826–4830.
Kong, D.S., Wang, H.T., Judy, J.C., Mauro, P., Kristie, J.K., Yao, J., Cui, Y., 2013. Nano Lett. 13, 1341–1347.
Li, C.X., Wang, H.Y., Shen, J., Tang, B., 2015. Anal. Chem. 87, 4283–4291.
Li, M., Cushing, S.K., Liang, H.Y., Suri, S., Ma, D.L., Wu, N.Q., 2013. Anal. Chem. 85, 2072–2078.
Li, N.X., Chen, J.Y., Luo, M., Chen, C.H., Ji, X.H., He, Z.K., 2017. Biosens. Bioelectron. 87, 325–331.
Li, X.L., Guo, J., Zhai, Q., Xia, J., Yi, G., 2016. Anal. Chim. Acta 934, 52–58.
Liu, X., Shuai, H.L., Liu, Y.J., Huang, K.J., 2016. Sens. Actuators. B 235, 603–613.
Patel, S., Patel, P., Undre, S.B., Pandya, S.R., Singh, M., Bakshi, S., 2016. J. Mol. Liq. 213, 304–311.
Retsinas, A., Kalampounias, A.G., Papatheodorou, G.N., 2016. J. Phys. Chem. Solids 99, 19–24.
Shuai, H.L., Huang, K.J., Chen, Y.X., 2016a. J. Mater. Chem. B 4, 1186–1196.
Shuai, H.L., Huang, K.J., Xing, L.L., Chen, Y.X., 2016b. Biosens. Bioelectron. 86, 337–345.
Trifonov, A., Sharon, E., Tel-Vered, R., Kahn, J.S., Willner, I., 2016. J. Phys. Chem. C 120, 15743–15752.
Tung, T.T., Yoo, J., Alotaibi, F.K., Nine, M.J., Karunagaran, R., Krebsz, M., Nguyen, G.T., Tran, D.N.H., Feller, J.F., Losic, D., 2016. ACS Appl. Mater. Interfaces 8, 16521–16532.
Wan, Y., Xu, H., Su, Y., Zhu, X.H., Song, S.P., Fan, C.H., 2013. Biosens. Bioelectron. 41, 526–531.
Wang, F., Elbaz, J., Orbach, R., Magen, N., Willner, I., 2011. J. Am. Chem. Soc. 133, 17149–17151.
Wang, G.J., Zhang, R.C., Xu, C., Zhou, R.Y., Dong, J., Bai, H.T., Zhan, X.W., 2014a. ACS Appl. Mater. Interfaces 6, 11136–11141.
Wang, H.T., Kong, D.S., Johanes, P., Cha, J.J., Zheng, G., Yan, K., Liu, N., Cui, Y., 2013. Nano Lett. 13, 3426–3433.
Wang, Q., Yang, C.Y., Xiang, Y., Yuan, R., Chai, Y.Q., 2014b. Biosens. Bioelectron. 55, 266–271.
Wang, Q., Li, Q., Yang, X.H., Wang, K.M., Du, S.S., Zhang, H., Nie, Y.J., 2016. Biosens. Bioelectron. 77, 1001–1007.
Wang, W.X., Ge, L., Sun, X.M., Hou, T., Li, F., 2015b. ACS Appl. Mater. Interfaces 7, 28566–28575.

Wang, X.Z., Ge, L., Yu, Y.F., Dong, S.S., Li, F., 2015a. Sens. Actuators B 220, 942–948.
Yao, W., Wang, L., Wang, H.Y., Zhang, X.L., Li, L., Zhang, N., Pan, L., Xing, N.N., 2013. Biosens. Bioelectron. 40, 356–361.
Ye, Y.D., Xia, L., Xu, D.D., Xing, X.J., Pang, D.W., Tang, H.W., 2016. Biosens. Bioelectron. 85, 837–843.
Yu, Y.Q., Wang, J.P., Zhao, M., Hong, L.R., Chai, Y.Q., Yuan, R., Zhuo, Y., 2016. Biosens. Bioelectron. 77, 442–450.
Yu, Y.Y., Chen, Z.G., Jian, W.S., Sun, D.P., Zhang, B.B., Li, X.C., Yao, M.C., 2015. Biosens. Bioelectron. 64, 566–571.
Yuan, R., Ding, S.J., Yan, Y.R., Zhang, Y., Zhang, Y.H., Cheng, W., 2016. Biosens. Bioelectron. 77, 19–25.
Zhou, W.J., Gong, X., Xiang, Y., Yuan, R., Chai, Y.Q., 2014. Biosens. Bioelectron. 55, 220–224.
Zhu, X., Wang, X.Y., He, F., Tang, F., Li, L.D., 2015. ACS Appl. Mater. Interfaces 7, 1334–1339.